final report

Project code: V.TEC.1718

Prepared by: Prof. Robert McLaughlin
The University of Adelaide

Date published: 1 February 2020

PUBLISHED BY
Meat and Livestock Australia Limited
Locked Bag 1961
NORTH SYDNEY NSW 2059

Rapid measurement of intramuscular fat in lamb using imaging needles

Meat & Livestock Australia acknowledges the matching funds provided by the Australian Government to support the research and development detailed in this publication.

Abstract

Intramuscular fat (IMF) is a key factor for achieving premium eating quality of lamb. There is no technology currently available to accurately and rapidly assess IMF in a commercial setting. We have developed an IMF needle that is able to measure IMF%. Scanning involves inserting a small needle containing a high-resolution imaging probe into the muscle. Our device uses a standard human medical imaging technology called optical coherence tomography. We have re-purposed this technology for uses in meat processing.

We were able to estimate IMF% values in cold loin samples with an accuracy of 1.1%. We were able to correctly identify almost three quarters of samples as low, medium or high IMF (71% accuracy). In warm carcases, were able to estimate IMF% with an accuracy of 1.4%.

Executive summary

- The sheepmeat industry currently has no practical methods to assess meat quality during processing.
- Developing a tool to measure intramuscular fat percentage (IMF%) would allow producers to optimise animal genetics and rearing techniques, allow processors to categorise carcases, and enable distributors to charge consumers a premium for high-quality products.
- Based on 10 years of university R&D, our team have developed an imaging needle. This is a highly miniaturised optical imaging probe encased within a small stainless steel needle (outer diameter 0.7mm).
- The imaging needle uses a standard medical imaging technology, optical coherence tomography, which is common in hospitals.
- The imaging needle was originally developed for human in vivo use, but we have repurposed it for applications in meat processing. It has the ability to distinguish between fat and muscle.
- In collaboration with researchers at the University of New England, we performed a pilot study on lambs being processed from the MLA Resource Flock (Tamworth, NSW).
- We were able to estimate IMF% from the needle scans of chilled samples. The average error in IMF estimate was 1.1%.
- We were also able to correctly categorise almost three quarters of samples as low, medium or high IMF (accuracy 71%).
- Within the limited scope of this study, we did not analyse the hot carcase data. However, we show that IMF is also visible in scans from the hot carcases.

Table of contents

1 Background

The percentage of intramuscular fat (IMF%) is a major determinant of eating quality in meat. An increase in IMF% has been shown to correlate with increased consumer perception of juiciness, flavour and overall liking (Thompson, 2004, Hopkins et al., 2006). Current methods to estimate IMF% typically involve freezing and homogenising a sample of the meat and then performing either chemical analysis or near infrared spectrophotometry (Perry et al., 2001). These methods are both time-consuming and destructive to the carcase, and cannot be incorporated into the meat processing workflow.

Optical coherence tomography (OCT) (Drexler and Fujimoto, 2015) is a high-resolution medical imaging technique that is commonly used in vivo in humans in hospitals. OCT is conceptually similar to ultrasound, but uses near infrared light instead of sound waves. We have re-purposed this technology for uses in meat production. OCT is able to acquire images of tissue microstructure that show a clear distinction between muscle tissue and fat deposits and has potential to quantify IMF%. However, the OCT signal is not able to penetrate deep into the body and can only image the superficial 1-2mm of muscle.

Our team have developed a solution to overcome this limitation, allowing us to acquire OCT images below the surface of the carcase. We have developed an **IMF needle**. This is a highly miniaturised OCT probe, encased within a hypodermic needle (Lorenser et al., 2015, Scolaro et al., 2012). The needle can be inserted deep into a carcase to acquire a real-time OCT measurement that shows muscle and fat to a depth of several centimetres. Fig. 1 shows our prototype IMF needle with an outer diameter of 0.7mm. This needle may be inserted into a carcase without leaving any perceivable mark, enabling rapid assessment of IMF%.

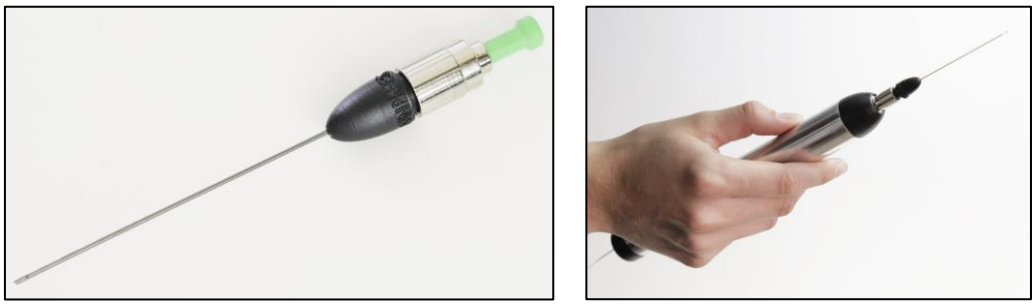

Fig. 1: (left) An IMF needle fabricated for this pilot study. (right) IMF needle attached to a hand-held mount.

2 Project objectives

The objectives of this project are to establish the feasibility of using IMF needle probes in meat production. The results of this project will provide a Go/No Go decision for the continuation of IMF needle technology to commercialization.

3 Methodology

3.1 Technology

Our team are one of a small number of research groups worldwide that have developed techniques to integrate an OCT imaging probe into a hypodermic needle. A schematic of a probe is shown in Fig. 2. Manufacture involves taking an optical fibre, the thickness of a human hair, and fabricating a sub-millimetre-scale lens at the imaging end of the fibre. This is then inserted into a stainless steel needle and carefully fixed in place with optical adhesive. Imaging is performed through a small imaging window that has been etched into the side of the needle. Our team have demonstrated the use of these imaging needles in a range of human applications from brain surgery to lung cancer (Ramakonar et al., 2018, Li et al., 2017). We are the first group to demonstrate their use in quantifying IMF% in meat production.

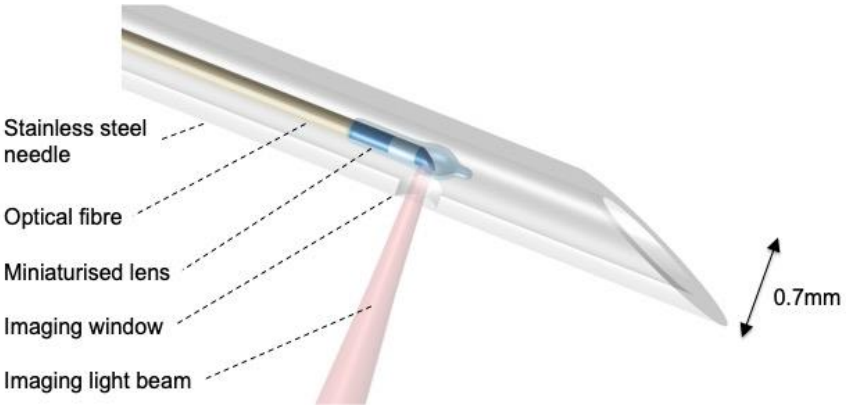

Fig. 2. Schematic of the IMF needle.

The IMF needle is integrated with an OCT scanner. These are available off-the-shelf from a number of international manufacturers (ThorLabs, Axsun, Lumedical Medical). The cost of an OCT scanner is roughly equivalent to an ultrasound scanner, typically ranging from AUD$15,000 – AUD$80,000. The prototype scanner and laptop used in this study are shown in Fig. 3. There is considerable scope to further miniaturise the scanner into a small backpack unit.

Fig. 3. OCT scanner and laptop used in pilot study.

3.2 Image Analysis

IMF needle scans may be acquired on hot or cold carcases. There is also scope to perform in vivo scans of animals during rearing, as our probes were originally designed for in vivo human use.

The optical properties of fat and muscle change as the meat is chilled. In chilled meat, the fat becomes opaque, appearing as small white regions. In the IMF needle scan, the fat appears as areas of high signal (light grey) on dark grey muscle tissue. Three representative scans are shown in Fig. 4-Fig. 6. The entire needle scan is shown at the top of each image, as the needle is withdrawn from the muscle. The length of each scan is approximately 20mm. Areas of intramuscular fat are highlighted in the zoomed insets shown below each scan.

Within the scope of this pilot project, we developed a technique to automatically quantify the percentage of intramuscular fat in chilled meat. The algorithm involved three steps. The scans were first spatially normalised to correct for variations in the speed at which the needle was moved by computing the rate of speckle decorrelation. The scans were then smoothed to remove noise using anisotropic diffusion. Finally, areas of fat were segmented using an adaptive threshold based on the average intensity within a moving window in the image.

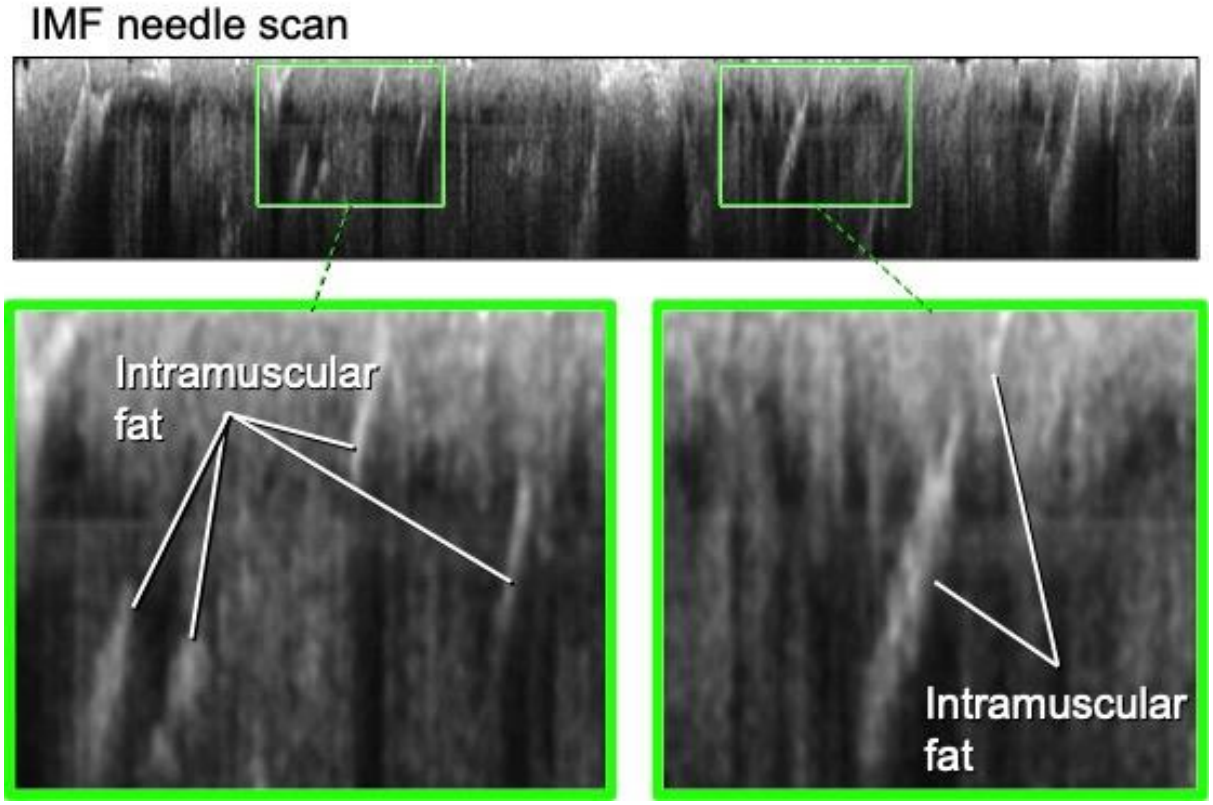

Fig. 4. Chilled sample 1. (top) IMF needle scan of chilled lamb loin sample. (bottom) Areas of intramuscular fat are highlighted in the insets.

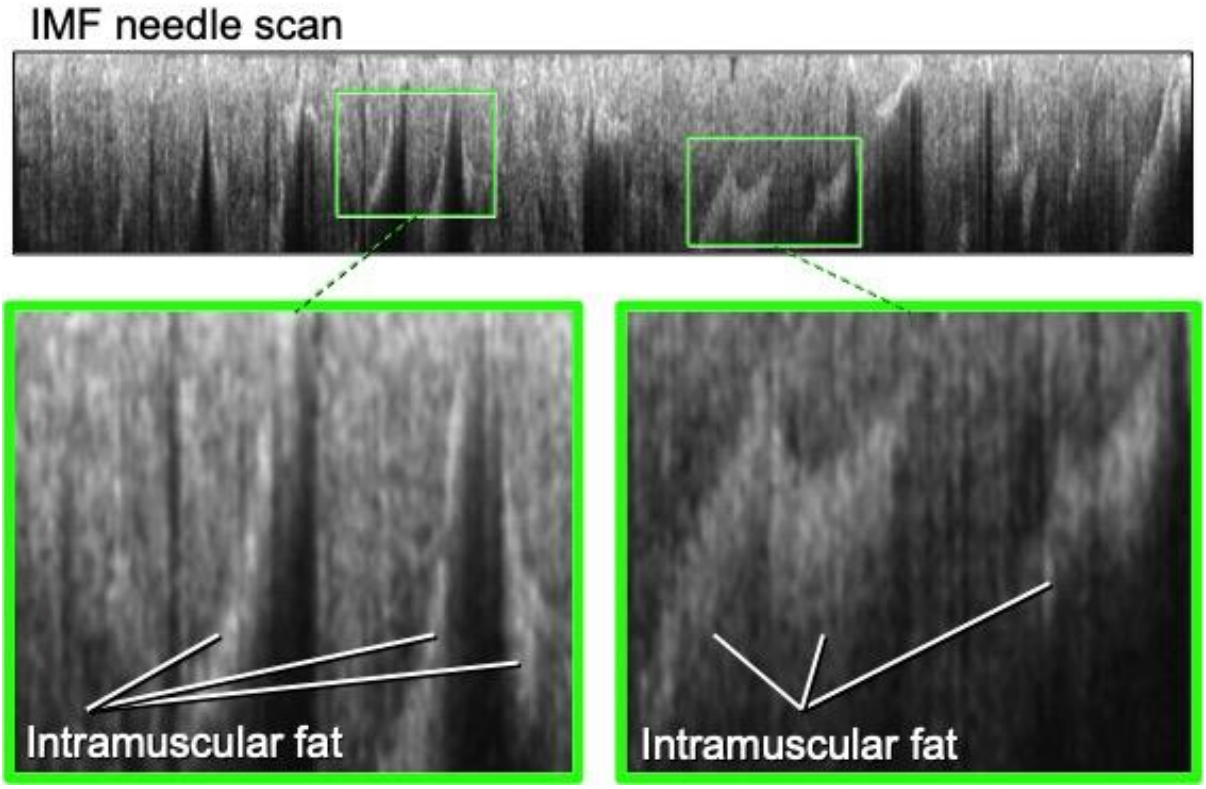

Fig. 5. Chilled sample 2. (top) IMF needle scan of chilled lamb loin sample. (bottom) Areas of intramuscular fat are highlighted in the insets.

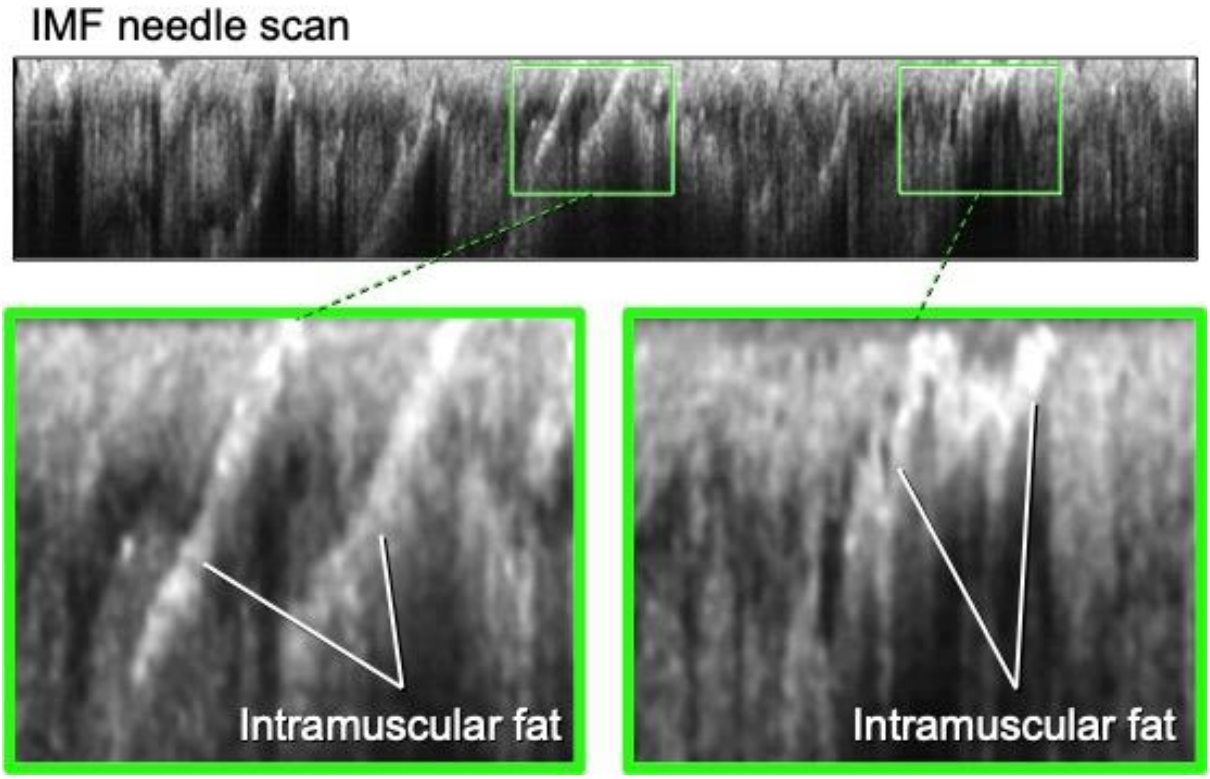

Fig. 6. Chilled sample 3. (top) IMF needle scan of chilled lamb loin sample. (bottom) Areas of intramuscular fat are highlighted in the insets.

Our team also acquired scans on several hot carcases, within 2 hours of slaughter. In these fresh samples, the fat has not solidified and is optically transparent, appearing as dark regions in the OCT scan. Because of the high resolution of OCT, individual fat cells are visible.

Within the limited scope of this pilot study, we did not develop automated image analysis algorithms to quantify the hot carcase scans. However, we were visually able to distinguish fat from muscle and such algorithms are feasible.

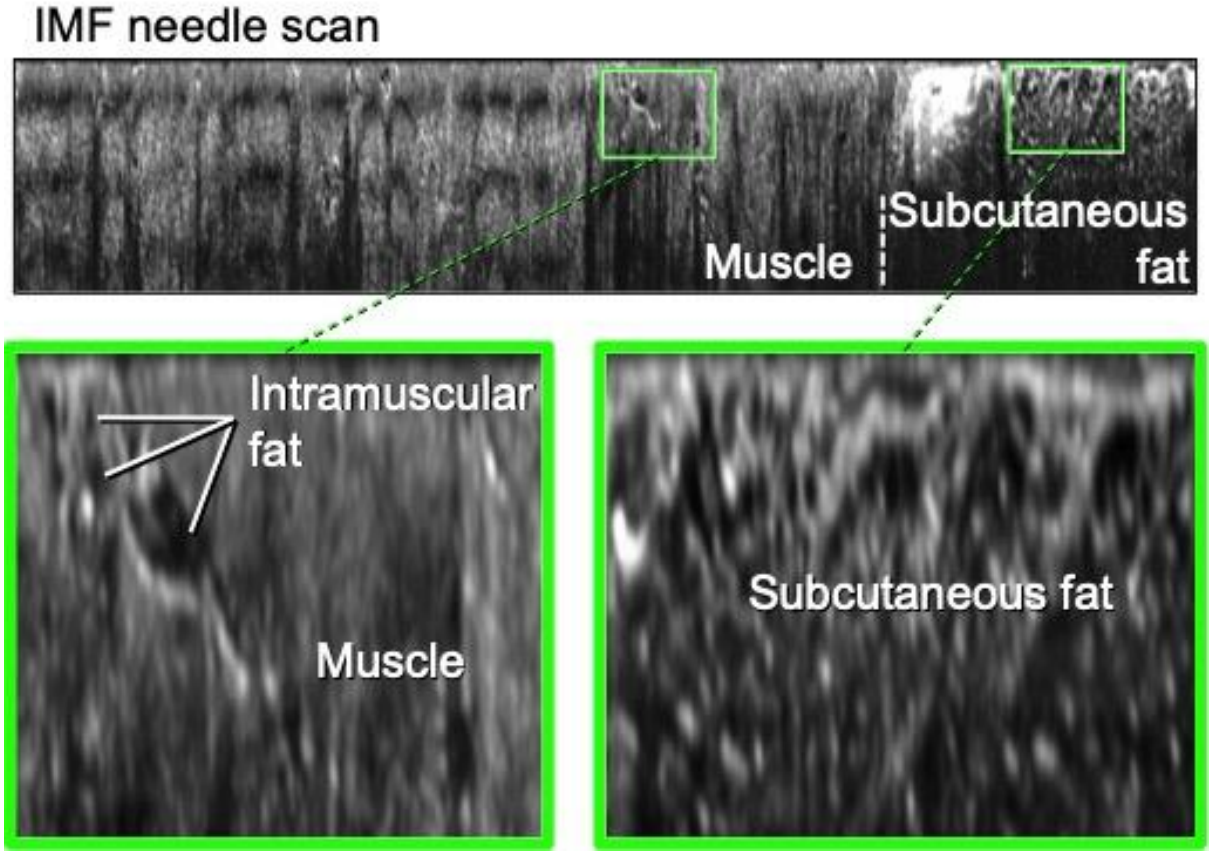

Fig. 7. Hot carcase sample 1. (top) IMF needle scan of fresh lamb loin sample. The tissue surface is on the far right of the image. Subcutaneous fat is visible on the right, while intramuscular fat is interspersed throughout the muscle on the left of the image. (bottom) Areas of intramuscular fat are highlighted in the insets.

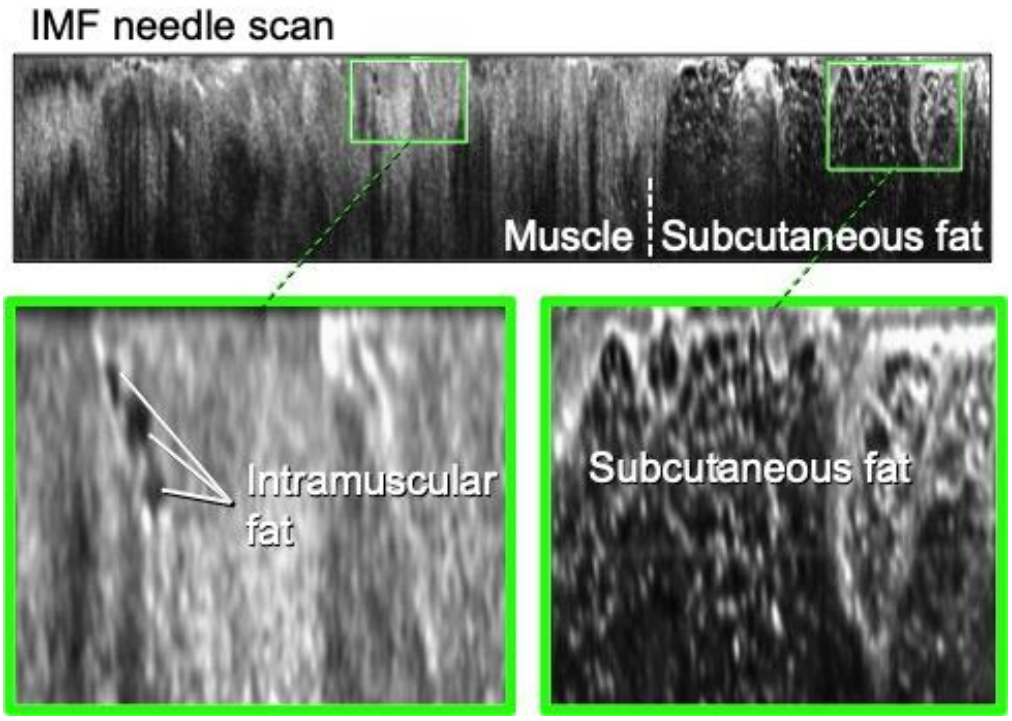

Fig. 8. Hot carcase sample 2. (top) IMF needle scan of fresh lamb loin sample. The tissue surface is on the far right of the image. Subcutaneous fat is visible on the right, while intramuscular fat is interspersed throughout the muscle on the left of the image. (bottom) Areas of intramuscular fat are highlighted in the insets.

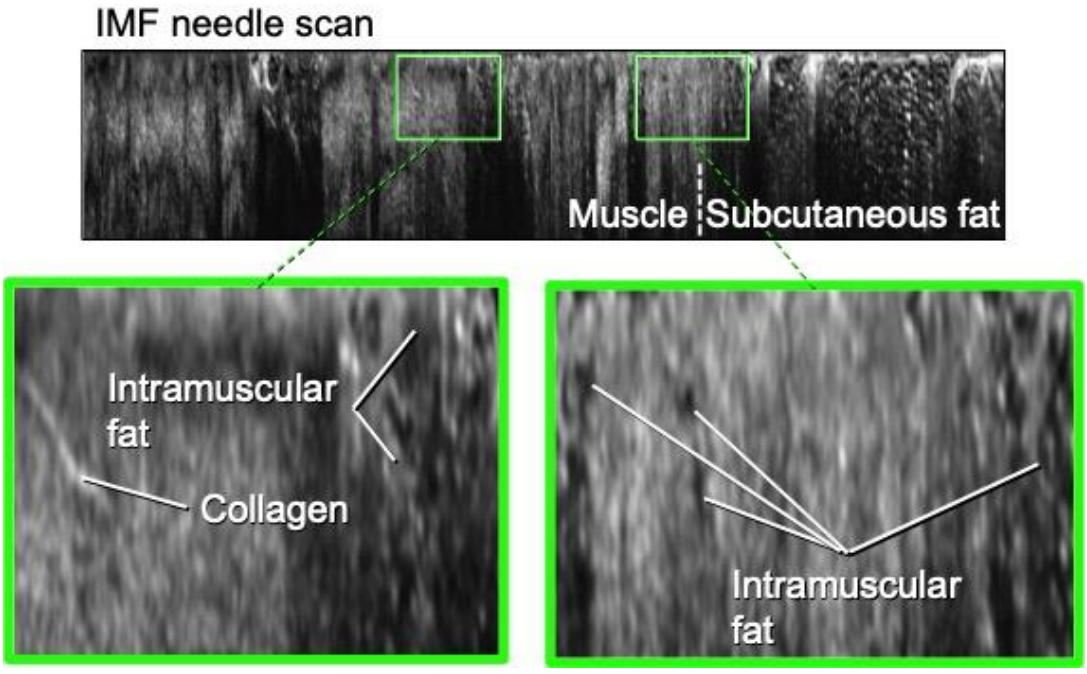

Fig. 9. Hot carcase sample 3. (top) IMF needle scan of fresh lamb loin sample. The tissue surface is on the far right of the image. Subcutaneous fat is visible on the right, while intramuscular fat is interspersed throughout the muscle on the left of the image. (bottom) Areas of intramuscular fat are highlighted in the insets.

3.3 Experiments and Analysis

Two hundred and fifty lambs from the MLA Resource Flock were processed at the Tamworth abattoir of Thomas Foods International as part of a larger study. Scans were acquired at 4 stages of processing:

- Hot carcases (0.5 – 2 hours post-slaughter): 30 scans
- Warm carcases (5 – 7.5 hours post-slaughter): 78 scans
- Cut sections (1 day post-slaughter, in the boning room): 250 scans
- Denuded loin samples (to be used for laboratory NIR IMF analysis) (2 days post-slaughter): 180 scans.

The denuded loins samples used for subsequent laboratory-based NIR IMF analysis were extracted from an area near the 12^{th} rib.

Image analysis of needle scans was performed on the denuded loin samples (2 days post-slaughter) and the warm carcases. The remaining scans have been archived for analysis in a future study.

Measurements using the IMF needle were compared against the gold standard values obtained from laboratory NIR analysis and statistically quantified by the R-value of the measurements. Accuracy was computed as the *average value of the absolute error in IMF% estimate*. For example, if the IMF needle estimated an IMF% of 4% and the gold standard value was 3%, then the absolute error would be 1%. IMF% accuracy was the average of this value computed over all data measurements. We have also calculated root mean square error (RMSE), slope and bias for these results.

In addition, we computed the accuracy with which the IMF needle could categorise samples as low, medium of high levels of IMF%. We defined three categories: low IMF (3% - 4.5%); medium IMF (4% - 6%); high IMF (5.5% - 12%). Note that the categories include a small amount of overlap as otherwise the error measure is inappropriately dominated by the samples that lie on the edge of each category. We report the percentage of samples assigned to a correct category.

Multiple needle insertions were performed on each sample. For the IMF samples (2 days post-slaughter), data was acquired from 10 needle insertions on each sample. For the warm carcases, 6 needle insertions were performed. For the IMF samples (2 days post-slaughter), we performed analysis to quantify the change in accuracy by reducing the number of needle insertions.

4 Results

4.1 IMF Accuracy

We were able to estimate IMF with an accuracy of 1.12% (average absolute error). IMF needle scans were performed on the denuded loin samples (2 days post-slaughter) that were to be sent for laboratory analysis. The estimate of IMF% was computed from 10 needle insertions on each sample. The results are shown in Figure 10. The R-value of the IMF Needle estimates is 0.418. The root mean squared error (RMSE) of the needle estimates is 1.38%. The slope of the line of best fit is 0.986 (with the y-intercept forced to zero). The bias of the results (i.e. error at mean of Gold Standard IMF values) is -0.08%.

We were able to distinguish between low, medium and high IMF levels with an accuracy of 71%.

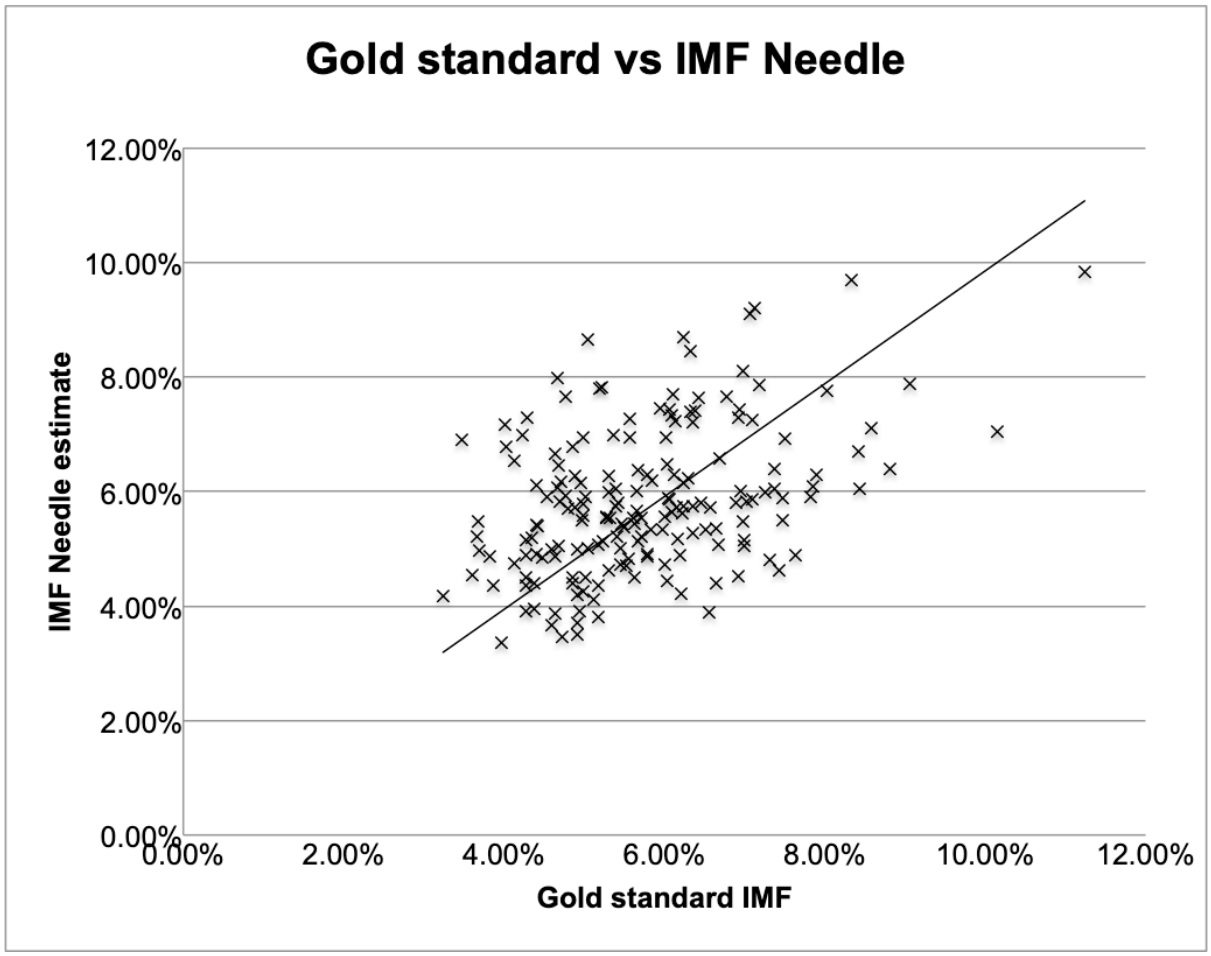

Fig. 10. IMF values, Gold standard vs IMF Needle estimate. Scans performed on denuded loin samples used for gold standard laboratory-based analysis, 2 days post-slaughter.

We were able to estimate IMF on the warm carcases with an accuracy of 1.40%. We acquired scans on the intact warm carcases 5 – 7.5 hours after slaughter whilst in the chiller room. Only 6 needle scans were acquired on each carcase. The IMF needle scans were taken near the left loin, but not on the exact area of muscle used for gold standard analysis. This resulted in more variation in the measurements. However, this only introduced a small, additional error in the average absolute IMF estimate. The estimates are plotted in Figure 11. The R-value is 0.38. The root mean squared error (RMSE) of the needle estimates is 1.76%. The slope of the line of best fit is 0.985 (with the y-intercept forced to zero). The bias of the results (i.e. error at mean of Gold Standard IMF values) is -0.09%.

In the warm carcase, we were able to distinguish between low, medium and high IMF levels with an accuracy of 63%. We used the same three categories as in the earlier experiment: low IMF (3% - 4.5%); medium IMF (4% - 6%); high IMF (5.5% - 12%).

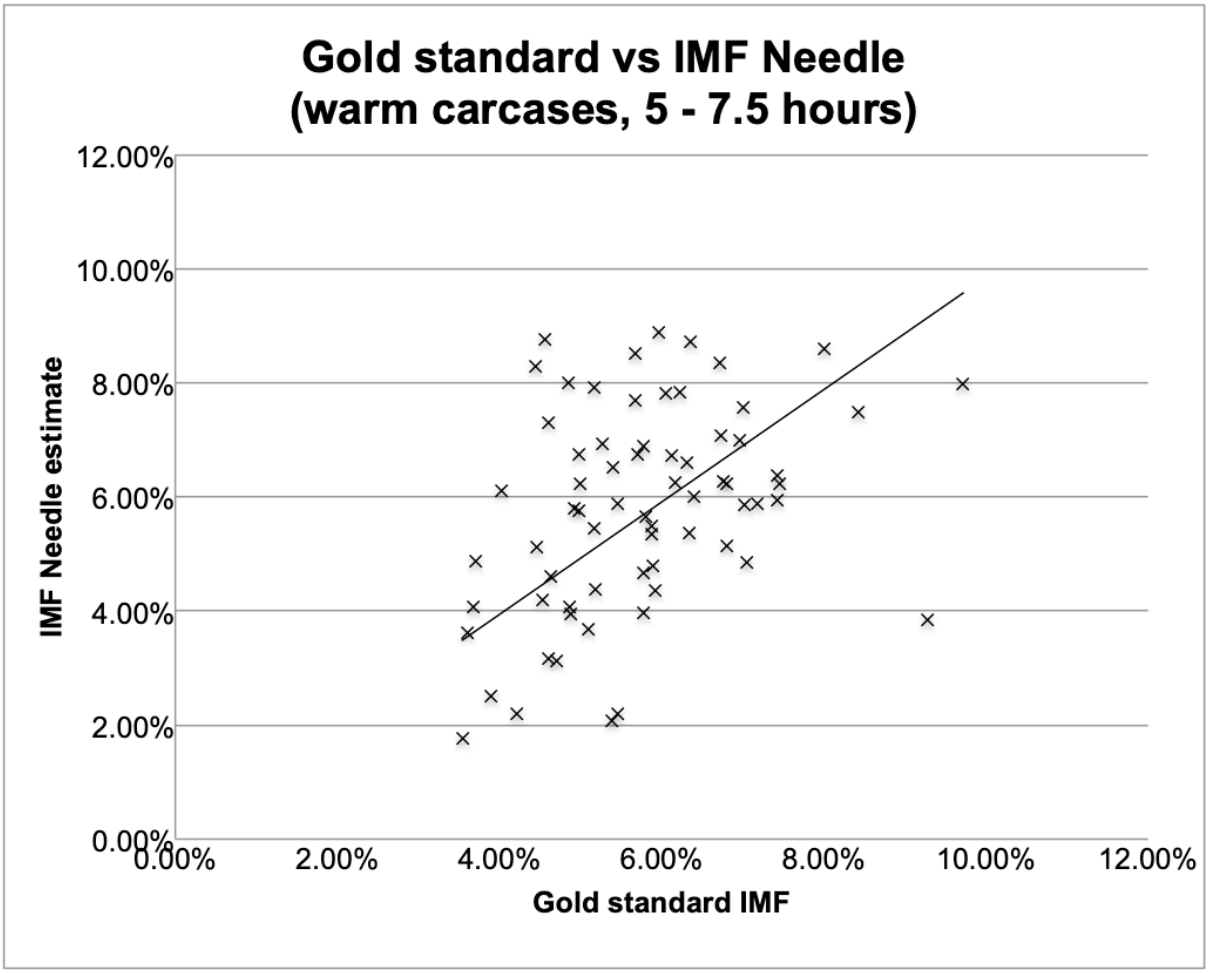

Fig. 11. IMF values, Gold standard vs IMF Needle estimate. Scans performed on warm carcases, 5 – 7.5 hours post-slaughter.

4.2 Impact of reducing the number of needle scans

We analysed the needle scan data on the samples that were sent for laboratory-based analysis, computing the accuracy using different numbers of needle insertions per sample. Accuracy is described in Fig. 12 for 2 – 10 needle insertions. IMF estimates were found to be more accurate with an increased number of needle scans. However, decreasing the needle scans had only a small impact on accuracy. The optimal value was 1.1% accuracy with 10 needle scans. However, reducing the number of needle scans to 4 needle scans still achieved an accuracy of 1.3%.

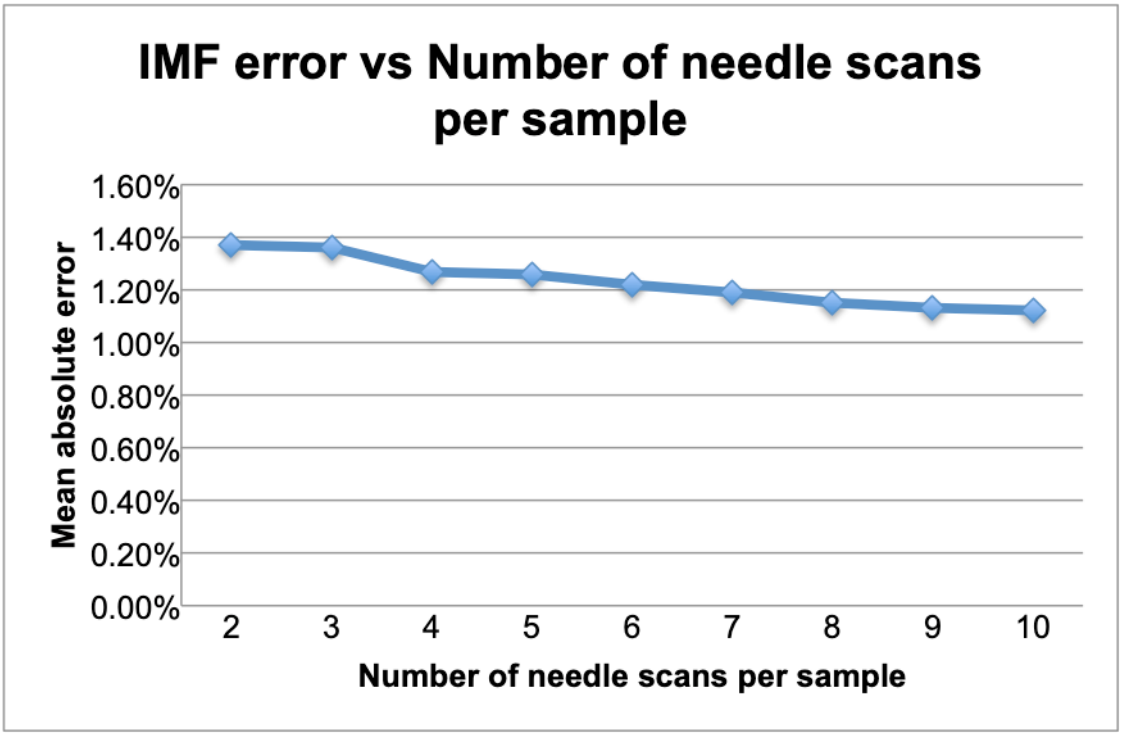

Fig.12. Change in IMF error with number of needle scans per sample (2-10 scans). Scans were performed on the denuded loin samples used for laboratory-based IMF analysis, 2 days post-slaughter. Mean absolute error is the difference between gold standard IMF% and needle estimate.

5 Discussion

This study has demonstrated the potential of the IMF needle to provide rapid assessment of IMF%. We have identified significant scope for further improvement in the results. Using standard image processing techniques, we were able to estimate IMF% with an accuracy of 1.1%. However, in recent years, deep learning algorithms based on artificial neural networks have proven to be superior to standard image processing techniques. Recent work by our group and others has demonstrated that deep learning algorithms are highly effective in the accurate analysis of OCT images (Yong et al., 2017, Abdolmanafi et al., 2017, Venhuizen et al., 2017). We anticipate that the IMF needle could achieve an accuracy better than 1% with the use of deep learning algorithms.

A range of other optical techniques have previously been explored for the estimation of IMF%. A limitation of all optical techniques is that light does not penetrate deeply into tissue, limiting these approaches to superficial measurements of IMF%, typically on a cut surface. These are inappropriate for use in an intact carcase. Our approach offers two critical innovations. Firstly, by encasing a miniaturised imaging probe within a needle we are able to measure deep below the surface of the carcase. Secondly, the probe performs continuous measurements during the entire needle insertion. This allows us to scan over a needle trajectory of 2-3 centimetres. This is critical for the accurate measurement of IMF% as the fat is not homogenously distributed throughout the tissue but instead occurs in small concentrations at a scale of 100s-of-microns to a few millimetres.

6 Conclusions/recommendations

6.1 Recommendations

The IMF needle has demonstrated sufficient accuracy to warrant the development of a commercial product. We recommend this be done in two stages. In Stage 1, the focus should be to resolve any technical issues with the design of the device. This includes modifying the device to perform more rapid scanning of a carcase, making the device portable and optimising IMF accuracy through the use of deep learning analysis algorithms. At completion, the goal of the Stage 1 project will be to deliver a minimal viable product that is appropriate for use in large-scale trials and also for initial commercial release to the industry. It would be most cost-effective to address these types of research & development tasks through a government leveraged funding scheme such as the ARC Linkage grant scheme.

In Stage 2, the focus would be on identifying manufacturing and distribution partners, scaling manufacture of the device, commercial roll-out and maximising the rate of industry adoption. This stage would be appropriate for commercial investment. To support the Stage 2 project stage, we recommend exploring Federal Government leverage schemes such as Accelerating Commercialisation, which offers up to $1mil in 1:1 leveraged funding.

7 Acknowledgements

We wish to sincerely thank the following people and organisations for their generous help in undertaking this pilot study: Peter McGilchrist (University of New England); Stephen Lee and Wayne Pitchford (University of Adelaide); Sam Hitchman (AgResearch, NZ); Max Noske and Son Country Meat; Bryden Quirk and Rodney Kirk (University of Adelaide).

8 Bibliography

ABDOLMANAFI, A., DUONG, L., DAHDAH, N. & CHERIET, F. 2017. Deep feature learning for automatic tissue classification of coronary artery using optical coherence tomography. *Biomedical Optics Express,* 8**,** 1203-1220.

DREXLER, W. & FUJIMOTO, J. G. 2015. *Optical coherence tomography : technology and applications,* Switzerland, Springer International Publishing.

HOPKINS, D. L., HEGARTY, R. S., WALKER, P. J. & PETHICK, D. W. 2006. Relationship between animal age, intramuscular fat, cooking loss, pH, shear force and eating quality of aged meat from sheep. *Australian Journal of Experimental Agriculture,* 46**,** 879-884.

LI, J., QUIRK, B. C., NOBLE, P. B., KIRK, R. W., SAMPSON, D. D. & MCLAUGHLIN, R. A. 2017. Flexible needle with integrated optical coherence tomography probe for imaging during transbronchial tissue aspiration. *Journal of Biomedical Optics,* 22**,** 1-5.

LORENSER, D., MCLAUGHLIN, R. A. & SAMPSON, D. D. 2015. Optical coherence tomography in a needle format. *In:* DREXLER, W. & FUJIMOTO, J. G. (eds.) *Optical coherence tomography: Technology and applications.* second ed. Switzerland: Springer International Publishing.

PERRY, D., SHORTHOSE, W. R., FERGUSON, D. M. & THOMPSON, J. M. 2001. Methods used in the CRC program for the determination of carcass yield and beef quality. *Australian Journal of Experimental Agriculture,* 41**,** 953-957.

RAMAKONAR, H., QUIRK, B. C., KIRK, R. W., LI, J., JACQUES, A., LIND, C. R. P. & MCLAUGHLIN, R. A. 2018. Intraoperative detection of blood vessels with an imaging needle during neurosurgery in humans. *Science Advances,* 4**,** eaav4992.

SCOLARO, L., LORENSER, D., MCLAUGHLIN, R. A., QUIRK, B. C., KIRK, R. W. & SAMPSON, D. D. 2012. High-sensitivity anastigmatic imaging needle for optical coherence tomography. *Optics Letters,* 37**,** 5247-5249.

THOMPSON, J. M. 2004. The effects of marbling on flavour and juiciness scores of cooked beef, after adjusting to a constant tenderness. *Australian Journal of Experimental Agriculture,* 44**,** 645-652.

VENHUIZEN, F. G., VAN GINNEKEN, B., LIEFERS, B., VAN GRINSVEN, M., FAUSER, S., HOYNG, C., THEELEN, T. & SANCHEZ, C. I. 2017. Robust total retina thickness segmentation in optical coherence tomography images using convolutional neural networks. *Biomedical Optics Express,* 8**,** 3292-3316.

YONG, Y. L., TAN, L. K., MCLAUGHLIN, R. A., CHEE, K. H. & LIEW, Y. M. 2017. Linear-regression convolutional neural network for fully automated coronary lumen segmentation in intravascular optical coherence tomography. *Journal of Biomedical Optics,* 22**,** 1-9.